Miniature Fuel Cells Fabricated on Silicon Substrates

S. C. Kelley, G. A. Deluga, and W. H. Smyrl
Dept. of Chemical Engineering and Materials Science, Corrosion Research Center, University of Minnesota, Minneapolis, MN 55455

Novel miniature fuel cells were fabricated from micromachined silicon wafers. The cells used methanol and air as reactants, and a thin polymer electrolyte as separator. The assembled cells had a working volume of 12 mm^3 and could be scaled down in size by three orders of magnitude by simple adjustments of the masking and etching procedures. Electrodeposition of Pt-Ru as the anode catalyst (oxidation of methanol) was successful in lowering the loading to 0.25 mg/cm^2 without loss of performance. Cell performance approached that of the best, state-of-the-art, large fuel cells, when scaled for size. In particular, single miniature cells yielded 822 Wh/kg and 924 Wh/L when operated at 70°C. The same chip design was also used for the hydrogen/air system, and the cell current, power, and specific energy density were higher than those of methanol/air. Further tailoring of the chips for specific fuels could lead to further improvements.

Introduction

Fuel cells can be thought of as chemical reactors which are designed to convert chemical reactant streams into electrical energy and chemical products. In recent years, a class of small reactors has emerged to carry out chemical reactions on a small scale (in volumes from 10^{-3} to 10^{-6} L). Reactor miniaturization has been accomplished by fabricating microreactors on inorganic substrates (such as silicon) using procedures developed by the microelectronics industry (photolithography, thin-film deposition, lift-off, and plasma-based etching). Microelectronic fabrication technology is ideal for the miniaturization of chemical systems because of its well proven cost-effectiveness, reproducibility, and control. By control, we mean the ability to design and fabricate structures with a high degree of precision (the resolution of photolithography is less than 1 μm) (Campbell, 1996).

Microchemical systems have inherent advantages over macrosystems, including increased rates of heat and mass transfer, increased safety as a result of smaller volume and enhanced temperature control, on-demand consumption or production of toxic reactants or products, reduced volume waste streams, and production scale-up by scale-out (the coupling of multiple microreactors instead of the use of one large reactor) (Jensen, 1999; DeWitt, 1999). Microreactor systems have been developed which contain an amazing variety of integrated microcomponents. A partial list includes: miniaturized heaters, mixers (Erfeld et al., 1999), filters (He et al., 1999), pumps, valves, reaction chambers, flow sensors, temperature sensors, and chemical analyzers (Jensen, 1999; DeWitt, 1999; Pantankar and Hu (1998). To date, microreactors have been used to: carry out reactions of commercial interest (Srinivasan et al., 1997; Burns and Ramshaw, 1999; Chambers and Spink, 1999; Hsing et al., 2000); analyze DNA (Burns et al., 1998); release controlled amounts of drugs (Santini et al., 1999); and fabricate microelectrodes *in situ* within a flow channel (Kenis et al., 1999).

The research cited shows that the adaptation of microelectronic fabrication techniques to microchemical systems can be successful. Thus, we have used microelectronic fabrication techniques in the present study to produce robust, miniaturized fuel cells. It is possible that this approach could be used to mass produce miniature fuel cells in the same way that integrated circuits are manufactured on silicon chips. Before describing the results, we compare miniature fuel cells to the existing alternate technology of miniature or micro batteries.

To compare miniature fuel cells to miniature batteries, one needs a basis (Vincent and Scrosati, 1997) related to the type of application being considered (for example, portable electronics). Specific energy (φ) is defined as the amount of energy deliverable from a device, per mass of the device (packaging plus reactants). This quantity is defined in Eq. 1

Table 1. Miniature Electrochemical Power Source Comparison

Cell Type	E (V)	i (mA/cm^2)	φ (Wh/kg)
Ni/Cd battery	1.2	10^{-1}	60
Ni/metal hydride battery	1.2	10^{-1}	65
$Li/Li_xMn_2O_4$ battery	3.0	10^{-1}	130
LiC_6/Li_xCoO_2 battery	3.6	10^{-1}	90
CH_3OH/O_2 m-PEFC	0.4	10^2	921

$$\varphi = I * E * t/m \tag{1}$$

where I is current, E is cell voltage, t is service time, and m is mass. Table 1 gives values of voltage, current density (i), and specific energy for several types of miniature electrochemical power sources based on performance values published in literature (Vincent and Scrosati, 1997; Baldauf and Preidel, 1999; Appleby, 1995; Bates et al., 1995; Powers, 1995; Jones et al., 1994).

All specific energy values in the table include device mass plus the mass of the reactants. The values for the miniature methanol/oxygen polymer electrolyte fuel cell (PEFC) are for a 10 h operation time using state-of-the-art performance numbers (0.1 A/cm^2 at 0.4 V and 60°C on 0.5M CH_3OH and ambient pressure air) (Baldauf and Preidel, 1999). The mass used to calculate the specific energy of the fuel cell includes the mass of the device (reactor) plus the mass of the fuel (methanol and water) consumed assuming 100% fuel utilization. The mass of oxygen is not included in the fuel cell specific energy calculation because it is obtained from the ambient atmosphere. The fuel cell mass and active-area used are the same as those for the miniature PEFC developed in the present investigation (0.0307 g and 0.25 cm^2).

As Table 1 shows, the specific energy of the miniature methanol/oxygen PEFC exceeds that of all miniature battery types by nearly an order of magnitude. Further, the miniature PEFC is able to deliver fuel cells over miniature batteries include ease of recharging (by adding liquid fuel), and lower emissions. The advantage of lower emissions comes about because fuel cells are superior in this respect to large power plants which supply the energy for battery recharging (Appleby, 1995; Amann, 1996). The one disadvantage of the miniature PEFC is its value of cell potential. Thermodynamically, a methanol/oxygen fuel cell should have a cell potential of 1.2 V. In practice, the cell potential is much lower (0.4–0.5 V) due to kinetic and ohmic limitations. Reports exist which propose goals, in terms of energy and power densities, for the application of miniature fuel cell systems as portable power sources (Amann, 1996; Datta and Smilanich, 1996). The miniature methanol/oxygen PEFC developed in the present study already meets many of the proposed goals. Thus, miniature fuel cells appear well suited to compete with miniature batteries as compact power sources for portable applications.

With the exception of a recent short publication by the present authors (Kelley et al., 2000), there appear to be no existing publications in the referred literature dealing with microfabricated, miniature polymer electrolyte fuel cells (hereafter denoted as m-PEFC). We note a recent publication on a miniature biofuel cell (Chen et al., 2001). Here, we survey publications which are related to the present subject. We have also listed (Wainright et al., 2000; Lee et al., 2000a, b; Maynard et al., 2000; Savinell et al., 2000; Meyers and Maynard, 2000; Hecht, 2000; Maynard and Meyers, 2000; Hebling, 2000) nonpublished work presented by other research groups on this topic.

Miniature fuel cells are mentioned by Savinell et al. in their work on oxygen reduction catalysts (both iron porphyrin and platinum based) (Gupta et al., 1998; Sun et al., 1998; Gojkovic et al., 1999a,b; Tokumitsu et al., 1999). Their cells consisted of flow channels machined in Teflon blocks to accommodate the testing of 1 cm^2 active area, conventionally prepared membrane electrode assemblies (MEAs). While small, the Teflon blocks were not microfabricated or suitable to serve as the basis for a miniature fuel cell power source.

Publications dealing with alternative PEFC designs, especially those that focus on planar schemes for connecting fuel cells in series, are also related to the topic of the present study (Dyer, 1990; Gottesfeld and Wilson, 2000; Adlhart et al., 1997; Heinzel et al., 1998; Barton et al., 1998a). Planar fuel cell stacks are well adapted to the volume constraints present for a miniature fuel cell power source. While little or no data has been published for a planar PEFC stack, from papers presented at recent conferences, we know that such designs are in the research stage prior to commercial development.

In addition, microelectronic fabrication techniques have previously been used to produce both electrochemical devices and microchemical systems (Campbell, 1996; Kovacs et al., 1994; Xia and Whitesides, 1998). Electrochemical devices include microelectrodes (used for electrochemistry investigations) (Kostecki et al., 1999; Buchler et al., 2000), thin-film lithium batteries (Jones et al., 1994; Bates et al., 1995; Li et al., 2000), and segmented current collectors fabricated on printed circuit boards (used to investigate the current distribution in fuel cells) (Rieke and Vanderborgh, 1987; Brown et al., 1992; Cleghorn et al., 1996; Wieser et al., 1998). Work on microchemical systems (microreactors) is described by Jensen (1999) and DeWitt (1999).

Finally, there is the application of small or miniature fuel cells as sensors (Barton et al., 1998b; Narayanan et al., 2000). Fuel cells can, in principle, be applied for the sensing of any reactant which can be used in a fuel cell (for example, alcohol, oxygen, and glucose). The application of fuel cells as sensors imposes many of the same size constraints as for miniature fuel cell power sources. We conclude this section by noting that, while related work exists, the design and testing of a microfabricated, silicon-based miniature methanol/oxygen PEFC remains a novel concept.

Experimental

Electrode chip fabrication

The m-PEFC electrodes were prepared on silicon using a series of fabrication steps adapted from Kovacs et al. (1994). Silicon was chosen as the fabrication material because of the wealth of information available pertaining to its processing, and its extensive use in microelectronic devices (Campbell,

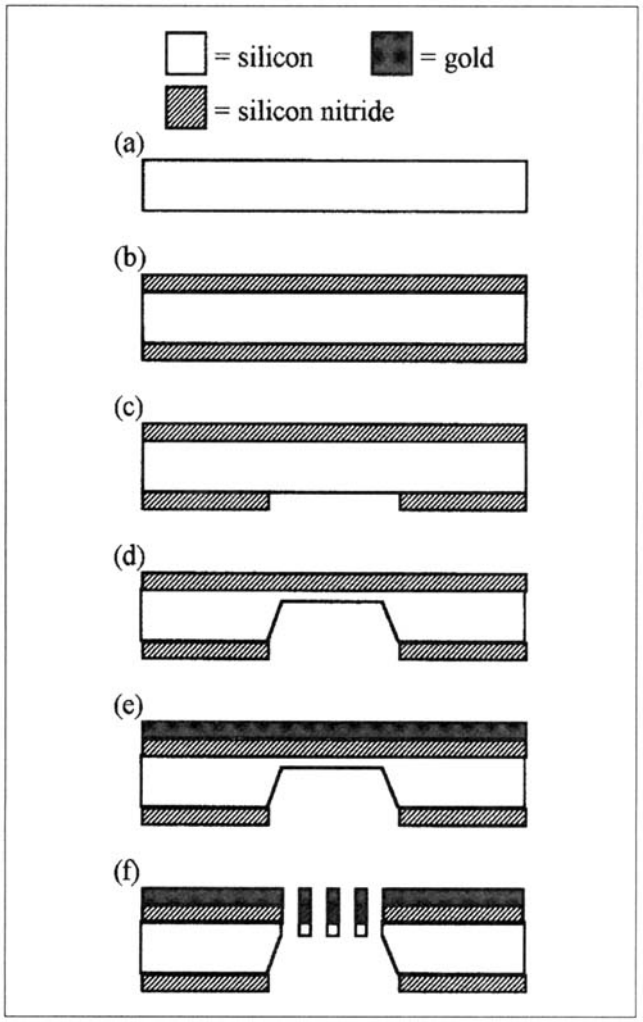

Figure 1. *m*-PEFC electrode fabrication steps.

(a) A bare, double-side polished silicon wafer; (b) grow LPCVD silicon nitride layers on wafer front and back; (c) pattern and etch window in silicon nitride layer on wafer back; (d) etch wafer in hot KOH solution to form silicon membrane; (e) pattern and deposit gold on wafer front; (f) pattern array of holes on wafer front and etch holes through gold, silicon nitride, and silicon membrane.

1996). Further, a clean room facility for the processing of silicon was readily available in the Electrical Engineering and Computer Science Dept. of the University of Minnesota. The fabrication process on silicon used in the present study is shown in Figure 1.

The starting material of choice was a 10 cm, $<100>$-oriented, double-side polished silicon wafer with a resistivity value $>10\ \Omega$ cm. First, low-pressure chemical vapor deposited (LPCVD) silicon nitride dielectric, Si_3N_4, was deposited on the wafer surfaces (Belyi, 1988) to act as an etch mask for the subsequent silicon wet etching. Next, using photo-lithographic patterning and subsequent plasma-based etching, windows were opened in the silicon nitride film on the back of the wafer. By etching the exposed silicon in a hot (90°C), aqueous solution of KOH (40 wt. %), the windows formed silicon membranes approximately 150 μm thick (Bean, 1978; Petersen, 1982; Matsuoka et al., 1992; Ristic et al., 1994).

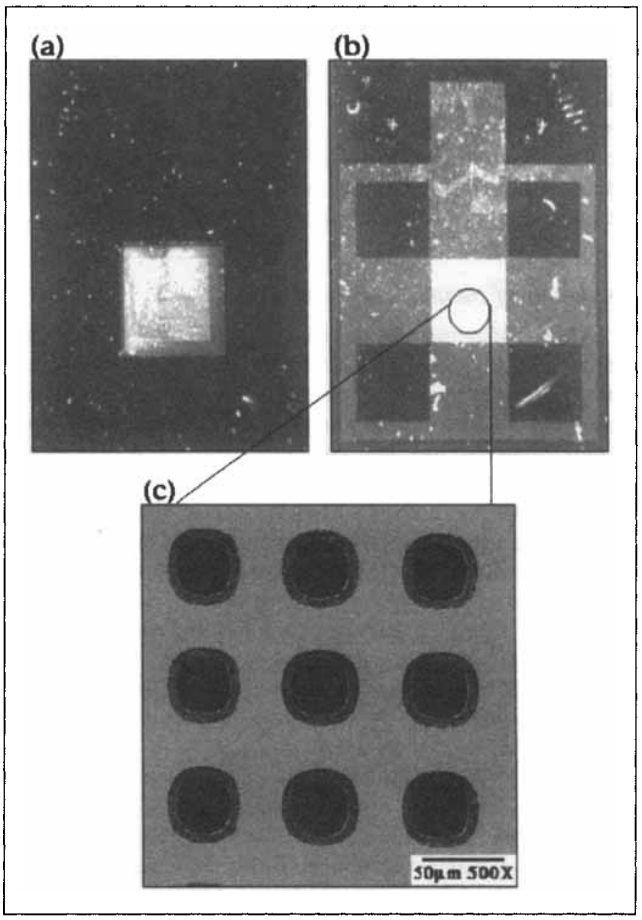

Figure 2. Micrographs of an *m*-PEFC electrode chip.

(a) Optical micrograph of the chip back; (b) optical micrograph of the chip front; (c) SEM micrograph close-up of the active-area with feedholes.

Next, using an additional photo-lithographic process, the front of the wafer was patterned and coated with gold to form electrodes. In a final photolithography step, an array of feedholes was patterned and etched through the gold layer using an iodine-based gold etch (Walker and Tarn, 1991). To complete the fabrication, the feedholes were then etched through the silicon nitride and silicon membrane using anisotropic, plasma-based etching (Cho et al., 1999). Individual m-PEFC chips were separated by manual cleavage of the finished wafers. The thickness of the gold film was 500 nm over a 15 nm titanium adhesion layer.

Figure 2 shows micrographs of the primary chip design used in the present investigation. The dark areas in Figures 2a and 2b are silicon nitride and the bright areas are the array of feedholes. The recessed area in Figure 2a serves as the flow-field for the methanol or oxygen being fed to the cell. The checker-board-shaped region in Figure 2b is the gold current collector. Figure 2c shows an SEM closeup of the gold current collector and of the array of feedholes on the chip front. In the SEM micrograph, the dark areas are the individual feedholes and the light areas are the gold between the holes. In order to maximize the electrode active area, the chips were fabricated such that the gold layer was deposited up to the edge of the feed holes. A single electrode chip is approxi-

mately 1.5 by 2.0 cm and 500–600 μm thick. The square array of feed holes, which is designated as the active area, is 0.5 cm on a side. The feedholes are nearly circular, 30 μm dia., and with an edge-to-edge hole spacing of 40 μm. The feedhole array shown in Figure 2 contains 5,184 feedholes. A fuel cell catalyst was applied to the feedhole array, which for the purpose of this investigation and for current density calculations, is considered to have an area of 0.25 cm^2.

Assembly of complete miniature cells

After fabricating the m-PEFC electrode chips, two such chips were combined with catalyst layers and a Nafion membrane in the typical bi-polar cell construction. The methanol electrode (anode) and oxygen electrode (cathode) were separately catalyzed and then combined with the Nafion membrane in a final assembly step.

The anode was prepared by electrodepositing Pt-Ru onto a carbon ink, previously spray-coated as a slurry onto the active area of an electrode chip. Spray-coating of the slurry was accomplished with an airbrush. The carbon ink was formulated as follows: 1.0 mg Ketjen black carbon (Lion) dispersed in 3.0 mL spray diluent (21 wt. % ACS grade isopropyl alcohol + 79 wt. % 18 MΩ DI water) by sonication. The ink was applied directly to an area 0.7 by 0.7 cm centered over the feedhole array on the front of the electrode chip.

Before Pt-Ru electrodeposition, the carbon-coated electrode chip active area was pre-treated by cyclic voltammetry in a three-electrode cell. The Pt-Ru electrodeposit for methanol oxidation was obtained from an aqueous solution containing the following: 1.0 M H_2SO_4 (ACS grade) + 0.016 M H_2PtCl_6 (Aldrich) + 0.008 M K_2RuCl_5 (Aldrich). Electrodeposition was carried out in a three-electrode cell using a potentiostat (EG&G PAR 173) to pulse the potential on the electrode chip to -0.05 V_{SCE}, followed by holding the potential at $+0.05$ V_{SCE}. The catalyst mass loading (mg/cm^2) was controlled by measuring the charge passed during electrodeposition on a digital coulometer. The actual mass loading was determined by chemical analysis. Electrodeposited anode chips were rinsed thoroughly with DI water to remove residual Cl^- ions, and allowed to dry before use in a cell.

The cathode was prepared in two steps by first spray-coating a Pt ink, and later by a Teflon-treated carbon ink (a diffusion layer), directly onto a Nafion membrane hydrated and protonated via the standard, published procedure (Parathasarathy et al., 1991; Ren et al., 1995). The Pt ink was formulated as follows: 2.0 mL spray diluent, 40.0 μL 5 wt. % Nafion (Aldrich), and 1.25 mg of unsupported Pt black (Johnson-Matthey). The Pt was dispersed in the liquid by sonication. This ink was applied by spray coating through a polymer mask (0.7 by 0.7 cm opening) centered on the Nafion membrane, drying with an ambient temperature air gun, and repeating the spray-dry cycle to achieve the final mass loading. The standard mass loading of Pt was 2.5 mg/cm^2 controlled by the mass of Pt added to the slurry.

After re-hydrating the Pt coated Nafion membrane in DI water overnight, a Teflon-treated carbon diffusion layer was applied directly over the Pt ink film of the cathode. The Teflon-treated carbon ink was formulated as follows: 1.0 mg XC72R carbon (Cabot), 1.0 mL of 18 MΩ DI water, and 1.0 μL of 30 wt. % aqueous Teflon dispersion (E-Tek). Again, the carbon was dispersed in the liquid by sonication. The carbon ink was spray-coated over the 0.7 by 0.7 cm Pt ink film, previously deposited on the Nafion, by alternately spraying and drying with an ambient temperature air gun. The completed cathode was hydrated overnight in DI water before use in a m-PEFC.

For direct comparison to the membrane electrode assembly in a typical PEFC, we also prepared anode and cathode catalyst layers where both were directly applied onto a Nafion membrane. The fabrication was started from a Nafion membrane already coated with Pt and Teflon-treated carbon ink films (as described above). The anode catalyst ink was formulated as for the cathode catalyst ink, with the substitution of JPL-type unsupported Pt-Ru black for the unsupported Johnson-Matthey Pt black (Surampudi et al., 1998) and applied to the Nafion membrane in a fashion analogous to that used for the cathode ink. Before use in a m-PEFC, the double-sided, catalyst coated Nafion membrane was hydrated in DI water overnight.

Assembly of the m-PEFC was achieved by stacking together the anode electrode chip, Nafion membrane, and cathode electrode chip. Lamination of the assembly was completed by hot-pressing at 30 psi and 170°C for 10 min., and then cooling in the press to ambient temperature under pressure. Before testing, insulated wire leads were soldered onto the exposed gold contact pads, and the cell assembly was allowed to hydrate overnight under DI water.

m-PEFC testing

Three types of m-PEFC results were obtained: fuel cell polarization, single electrode polarization, and methanol crossover. Fuel cell polarization experiments were carried out by scanning the cell potential at 0.001 V/s and measuring the current produced. By means of a saturated calomel reference electrode (SCE; Fisher, Accumet) electrode potentials of the anode and cathode vs. the SCE were measured concurrently during this experiment. We identify these measurements as single-electrode measurements in the discussion to follow. Methanol crossover rate measurements were carried out by using an infra-red absorption analyzer (Rosemount Analytical) to measure the carbon dioxide concentration in the oxygen electrode exhaust, while fixing the fuel cell potential and measuring the current. The results of the above three tests will be used, as appropriate, in the discussion to follow.

The variables which were explored in this investigation are as follows: temperature, Nafion thickness, and oxygen concentration. In the course of relating the effect of each of the above variables to methanol/oxygen m-PEFC performance, unique aspects of the cell developed in the present study will be revealed.

Results and Discussion

Electrode chip design

Figure 3 gives SEM micrographs of the active areas of the three different electrode chip designs tested during the present investigation. At the center of the problem of electrode chip design was the manner in which to distribute active area and feed holes. The first design (Figure 3a) was a series of feed holes within a coil of gold wire, 5 μm in width. It was discarded because it used a long, single path for elec-

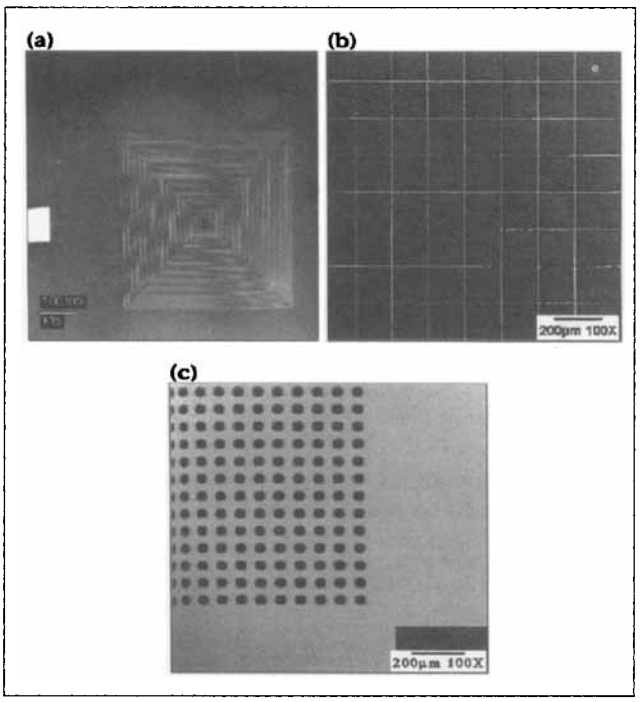

Figure 3. Three *m*-PEFC electrode chip designs studied.

SEM micrographs. (a) Coil design, (b) wire grid design; (c) feedhole array design. Dark areas are silicon nitride coated silicon. Bright areas are gold, thin-film electrodes. A feedhole array is present only in (c), dark areas within gold electrode.

tronic conduction which was fragile and highly resistive. The second design (Figure 3b) was dismissed because much of the possible active area (the space between the wires and feedholes) was wasted. The final and most successful electrode chip concept (Figure 3c) placed the same array of feedholes within a planar gold electrode. This design was advantageous, because it maximized the active area and had multiple, low ohmic resistance electronic pathways.

Figure 2 shows micrographs of the final electrode chip design used in the present study. Feedhole and rib size were the primary variables in this electrode chip design, and the size shown here was held fixed for the present study. The sizes used here insured excellent liquid/gas handling in the individual electrodes. Varying each of the variables could be expected to have profound effects on methanol crossover, catalyst utilization, and cathode flooding. These are the subjects of ongoing studies and the results will be reported in subsequent articles. The above listed feedhole and rib sizes gave a total feedhole area of 0.0467 cm^2 and a total rib area of 0.203 cm^2. It should be noted that the current densities quoted below are actually larger due to the reduction of gold electrode area because of the feed holes (0.203 cm^2 vs. 0.25 cm^2).

Thus, the chip design developed in the present study is simple and compact. The current design could be further simplified by depositing the polymer electrolyte (or another form of proton conductor) directly on one or both of the electrode chips, thereby eliminating the need for a separate polymer electrolyte membrane. However, the design described here is quite successful in that it allows the exploration of the effects of a wide variety of design variables on cell performance.

Catalyst configuration on the individual electrodes

In the course of the present investigation, there were several different types of methanol/oxygen cells tested, each distinguished by its particular type and combination of catalyst layers. The various combinations are listed in Table 2 for illustration of the range of study, but further discussion of them will be reserved for a companion article on catalysis of methanol oxidation, to be published shortly. The best system (cell type D) was an electrodeposited Pt-Ru anode catalyst supported on carbon (anode) and Pt catalyst ink spray-coated on the cathode membrane combined with a carbon "diffusion layer" (cathode side).

We compare the performance of cell (D) with (E) in Figure 4. In cell (E), the catalyst layers on both electrodes were inks deposited directly onto the Nafion membrane. It can be seen that m-PEFC configuration (D) was superior to (E) over the entire potential range of the polarization curve. That is, a greater cell current was produced by (D) at all values of cell potential. The reason for this can be better explained by considering the single electrode measurements (see Figure 5).

Since the cathode catalyst layers of cells (D) and (E) were identical, it was expected that the cathode polarization curves

Table 2. *m*-PEFC Configurations and Catalyst Mass Loading*

Designation	Anode Type	Anode Loading (mg/cm^2)	Cathode Type	Cathode Loading (mg/cm^2)
A	Planar edep. (on chip)	1.56 (Pt-Ru, 79: 21)	Planar edep. (on chip)	137 (100% Pt)
B	Planar edep. (on chip)	1.56 (Pt-Ru, 79: 21)	Sprayed ink (on chip)	5.0 (JM Pt black)
C	Planar edep. (on chip)	1.60 (Pt-Ru, 88: 12)	Sprayed ink (on Nafion)	2.5 (JM Pt black)
D	KJB edep. (on chip)	0.25 (Pt-Ru, 85: 15)	Sprayed ink (on Nafion)	2.5 (JM Pt black)
E	Sprayed ink (on Nafion)	2.5 (JPL Pt-Ru black)	Sprayed ink (on Nafion)	2.5 (JM Pt black)

*The different m-PEFC configurations will be referred to by the designations given below.
Anode = methanol electrode (Pt- Ru alloy).
Cathode = oxygen electrode (Pt).

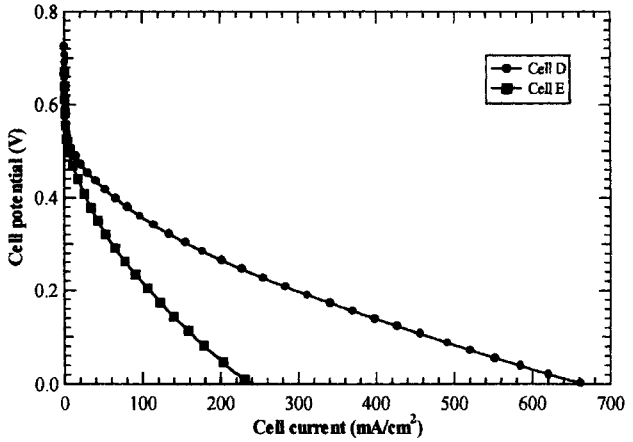

Figure 4. Influence of catalyst configuration on cell performance.

(D) Electrodeposited anode catalyst; (E) spray-coated JPL catalyst ink. 0.2 L/min. 0.5 M aqueous methanol fuel at 70°C; 0.2 L/min. ambient air; Nafion 117.

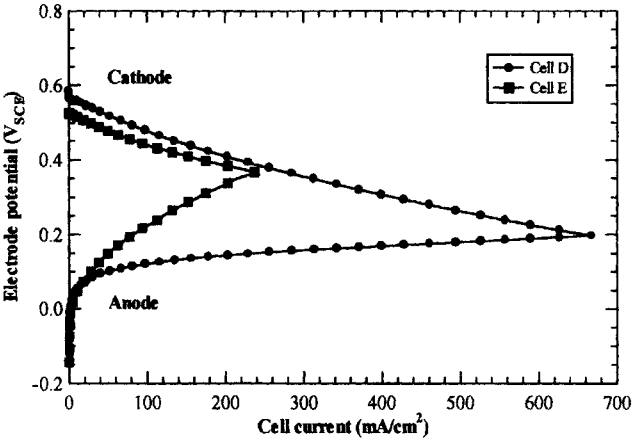

Figure 5. Influence of catalyst configuration on single electrode performance.

(D) Electrodeposited anode catalyst; (E) spray-coated JPL catalyst ink. 0.2 L/min. 0.5 M aqueous methanol fuel at 70°C; 0.2 L/min. ambient air; Nafion 117.

in Figure 5 should be the same. However, it was found that the *anode* of (D) was superior to that of (E). This is shown in Figure 5, where, for any given value of current, anode (D) had a lower potential (smaller driving force) than anode (E). Thus, despite the mass loading of anode (D) being about an order of magnitude less than that on (E), the anode and, therefore, the cell performance of cell (D) was superior to the conventionally catalyzed cell (E). This result highlights the benefit of using the electrodeposited anode catalyst developed in the present study.

Temperature, membrane thickness, and oxygen concentration

The experiments performed to evaluate the effect of temperature on m-PEFC performance were accomplished by changing the temperature of the aqueous methanol feed. A methanol concentration of 0.5 M was used for all temperatures evaluated, and the flow rates of both reactants (methanol and air) were 0.2 L/min. at ambient pressure. Figure 6 shows the results of cell polarization at the three temperatures tested (23, 50, and 70°C). As expected, in terms of output current, the performance at all values of cell potential increased with temperature. However, the increase from 23 to 50°C was much greater than the increase from 50 to 70°C. An increase in temperature improved cell performance due to improved rates of reaction and of mass transport on each fuel cell electrode. Unfortunately, as will be seen, methanol crossover rates also increased with temperature. For a fuel cell to experience a net increase in performance with temperature, the positive effects of increased mass transport and reaction rates must be greater than the negative effect of increased methanol crossover.

From the single electrode measurements (not shown), it was concluded that the majority of the increase in performance of the m-PEFC with temperature was due to an increase in the performance of the anode. On the other hand, the cathode performance at 50°C was only marginally superior to that at 23°C, but the performances at 23°C and 70°C were the same. Thus, the increase in cell performance from 50 to 70°C was small. The increase in the methanol crossover rate with temperature is shown clearly in Figure 7.

Changing the thickness of Nafion in a methanol/oxygen PEFC is expected to have two effects. First, the ohmic of the polymer electrolyte membrane (PEM) increases with thickness. Second, the magnitude of the methanol crossover rate scales inversely with the PEM thickness. The first effect tends to improve PEFC performance for a decrease in PEM thickness, while the second does the opposite. In order to evaluate the influence of membrane thickness, a different miniature cell was assembled for each thickness. The different cells were of the same design and identical in all other respects. The effect of Nafion thickness on performance was evaluated using 0.5 M aqueous methanol fuel at 70°C. The Nafion (1,100 equivalent weight) thickness values tested were 2, 4, 7, and 9 mil (50.8, 101.6, 177.8, and 228.6 μm).

Figure 8 shows the results for simultaneous measurement of m-PEFC polarization and methanol crossover rate. As can

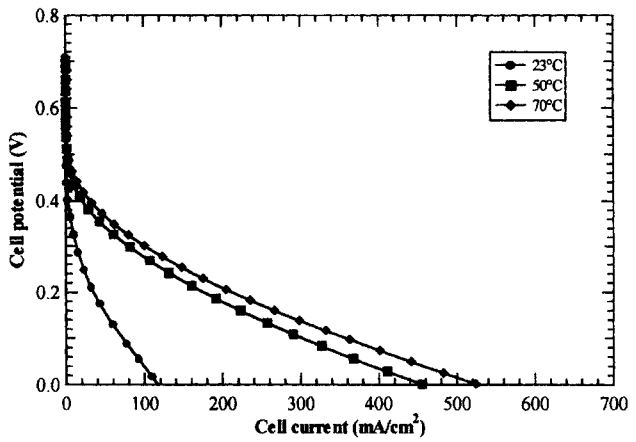

Figure 6. Effect of temperature on cell performance.

0.2 L/min. 0.5 M aqueous methanol fuel at specified temperatures; 0.2 L/min. ambient air; Nafion 117.

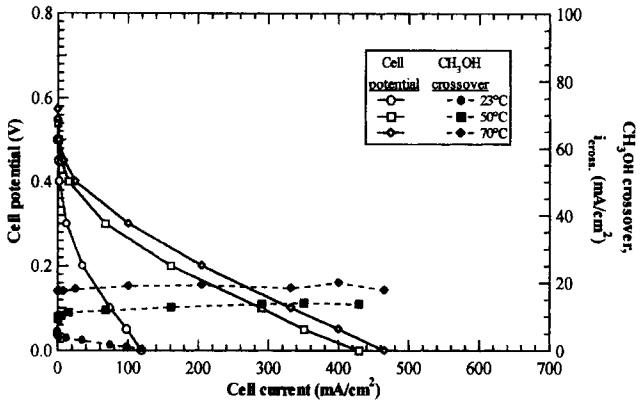

Figure 7. Effect of temperature on methanol crossover.

0.2 L/min. 0.5 M aqueous methanol fuel at specified temperatures; 0.2 L/min. ambient air; Nafion 117.

be seen from the plot, at low values of cell current (high cell potential), the cell behavior was dominated by methanol crossover, so the cell performance decreased with decreasing Nafion thickness. However, as the cell current increased, the cell with the thinnest Nafion performed best. This was due to the dominant influence of Nafion ohmic resistance.

To determine the influence of oxygen concentration on cell performance, we switched from air (21% oxygen) to neat oxygen. As might be expected, increasing the concentration of oxygen in the cathode feedstream from 21 to 100% appreciably improved the overall performance. It is generally accepted that the kinetic rate of oxygen reduction has a first-order dependence on oxygen concentration. Thus, in going from air to oxygen (which increased the oxygen concentration by roughly five times), we would expect a kinetically controlled oxygen reduction current to increase by the same factor. The data in Figure 9 show that at high values of cell potential, the cell current at a given potential for pure oxygen (vs. air) was indeed close to five times greater. However, as the cell current increased, this factor decreased to less than two.

The smaller than expected current increase with oxygen concentration was caused by methanol crossover as indicated

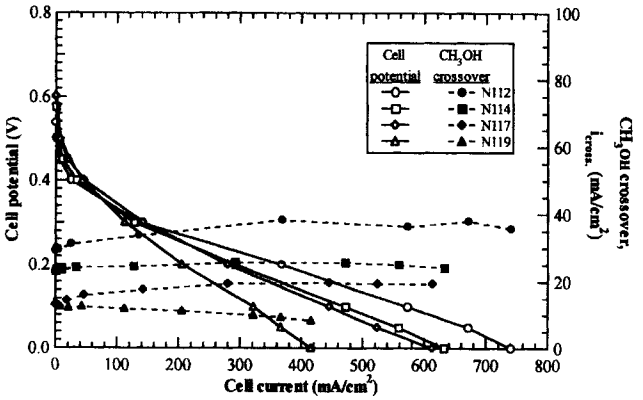

Figure 8. Effect of Nafion thickness on cell performance and methanol crossover.

0.2 L/min. 0.5 M aqueous methanol fuel at 70°C; 0.2 L/min. ambient air; specified values of Nafion thickness.

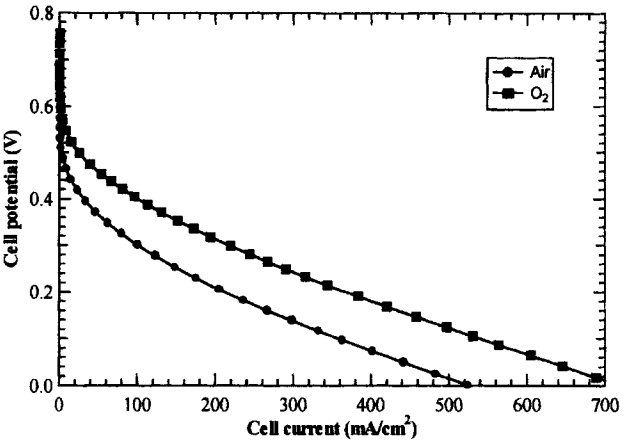

Figure 9. Effect of oxygen concentration on cell performance.

0.2 L/min. 0.5 M aqueous methanol fuel at 70°C; 0.2 L/min. ambient air or oxygen; Nafion 117; OCP to 0 V_{cell} at 0.001 V/s.

by the poor performance of the cathode in single electrode polarization curves. At low cell currents, the cathode was able to handle the rate of methanol crossover, and its behavior was controlled by oxygen reduction kinetics. At high cell currents, due to the amount of methanol arriving at the cathode, the kinetic control became mixed between the two reactions. Thus, the apparent reaction order changed.

Methanol crossover

We have measured the rate of methanol crossover for the miniature cell configuration, and the results have been plotted in the preceding figures. In Figure 10, the measured crossover rate (expressed as a current density) has been plotted vs. the rate calculated as described below. All of the data in Figure 10 are given for zero current conditions, and only reflect the influence of diffusion across the membrane, that is, the effect of electroosmotic drag is not included. The measurements were carried out as a function of membrane thick-

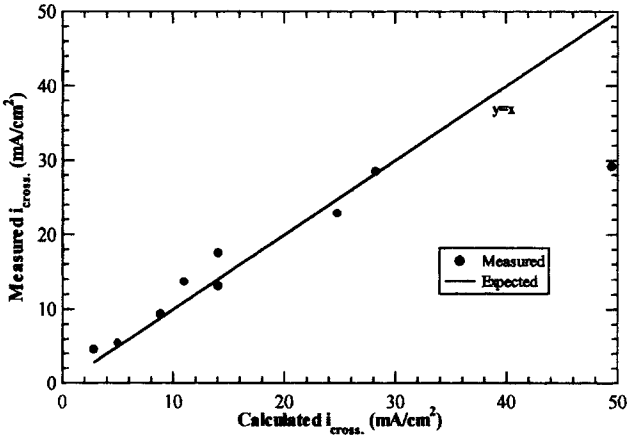

Figure 10. Measured crossover rates at open circuit compared to calculated values for all electrolyte thicknesses, solution concentrations and temperatures used here.

ness, methanol concentration, and temperature. It can be seen that the calculated values match the measurements rather well. In order to estimate the rate of diffusion across the membrane, the diffusion coefficient (D) was assumed constant with thickness, and it was taken from the literature along with the partition coefficient (H) of methanol in water and Nafion at all concentrations and test temperatures. The rate of crossover was calculated according to the relationship

$$i_{\text{crossover}}(\text{calculated}) = nFDH(A_{fh}/A_{\text{active}})\Delta C/\Delta x \quad (2)$$

where A_{fh} is the area exposed through the feed holes, A_{active} is the total area (0.25 cm^2), Δx is the membrane thickness, F is the Faraday constant, n is the number of electrons involved in the reaction ($n = 6$), and

$$\Delta C = C_{\text{feed}} - C_{\text{cathode}} = C_{\text{feed}} \quad (3)$$

The latter relationship is used because all the methanol that crosses over is consumed at the cathode. It is important to note that the correction for area must be made in order to get agreement between measured and calculated crossover rates. It is clear from the data shown in the previous figures that, at non-zero current density, methanol is also transported across the membrane by electroosmotic drag, and the crossover rate is increased. Further analysis of crossover will not be done here, but it is an area of active interest. We are studying other membranes in order to reduce the crossover rate and results will be published in subsequent articles.

Comparison with large cells

Figure 11 shows the polarization results for a miniature cell at 70°C operating on 0.5 M methanol using a Nafion 117 membrane. The m-PEFC at 70°C produced approximately 70 mA/cm^2 at 0.4 V_{cell}, with a peak power output of 15 mW at 0.2 V_{cell}. The cell had a mass of 0.031 g and a volume of 0.012 cm^3. Using the above performance results, we calculated the energy density and specific energy to be 924 Wh/L and 822 Wh/kg, respectively. These values include the volume or mass of the methanol and water consumed during a 10 h operating time, but neglect methanol loss due to crossover. The above value for specific energy favorably compares to the state-of-the-art value in Table 1.

We now turn our attention to the comparison of the m-PEFC results with those for previously published large methanol/oxygen PEFCs. Comparison will be made on the basis of cell polarization, single electrode polarization. Table 3 relates the test conditions used for all fuel cells compared (large and miniature). Not all of the cells shown in the table were used for every comparison. Those omitted provided no applicable data for the given comparison. Where possible, data were chosen which originated from test conditions (temperature, pressure, reactant concentration, Nafion thickness, and catalyst loading values) that closely matched those used for the m-PEFC. The cells listed in Table 3, besides the in-

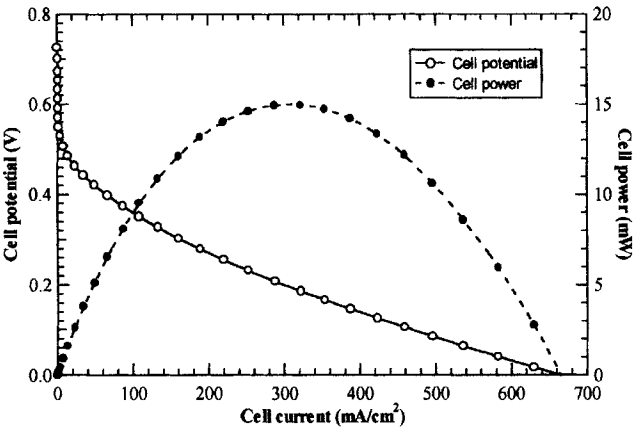

Figure 11. Performance and power of miniature cells at 70°C.

0.2 L/min. 0.5 M aqueous methanol; 0.2 L/min. ambient air; Nafion 117.

house large PEFC and m-PEFC results, were taken from the publications cited. A question mark entry in the table indicates a test condition for which no data was provided.

Figure 12 compares the fuel cell polarization curves for select cells listed in Table 3 (as indicated by the legend). As can be seen in the figure, the m-PEFC results compared well to those for the published and in-house large PEFCs. For most values of cell potential, the m-PEFC cell current was within a factor of three (two in most cases) of that produced by the large PEFCs. Certainly, the results of Arico et al. and Baldauf and Preidel are exceptional. Otherwise, the m-PEFC results were equivalent or only slightly below those for the large PEFCs.

In making comparison of m-PEFC to large PEFC performance, there were only three sets of published large PEFC data which gave single electrode measurements. These cells are indicated in the legend of Figure 13. The anode polarization curves revealed that the m-PEFC anode was equivalent to those of the large PEFCs. This equivalence came about despite the fact that the electrodeposited Pt-Ru anode mass loading in the m-PEFC was nearly an order of magnitude lower than that on the large PEFC anodes. Thus, the difference in performance between the m-PEFC and the large PEFCs was due to the difference in cathode performance. Two of the three sets of large PEFC results in Figure 13 originated from cells with a much higher cathode Pt mass loading than on the m-PEFC cathode (6 and 12 mg/cm^2 vs. 2.5 mg/cm^2). Only the cell of Ren et al. had a similar Pt loading (1.2 mg/cm^2). Thus, at least part of the reason that the m-PEFC cathode showed lower performance (in terms of potential at a given cell current) was Pt mass loading.

Miniature hydrogen/oxygen fuel cells

Up to this point, only the results for methanol/oxygen as reactants have been reported. To illustrate the flexibility of the chip design, we also tested an m-PEFC fueled by neat hydrogen and air. Since a hydrogen/oxygen fuel cell system has inherent problems with water management, the hydrogen gas was humidified at 30°C before being fed to the cell; how-

ever, the cell operated at room temperature (23°C). The hydrogen/oxygen cell was constructed using a Nafion 112 membrane spray-coated with 2.5 mg/cm^2 Pt black for the oxygen electrode (cathode). The hydrogen electrode (anode) was made from 1 mg/cm^2 Pt electrodeposited on a spray-coated ink of Ketjen black carbon ink on the anode chip. The hydrogen/oxygen mini-cell was assembled by the same procedure as for the methanol/oxygen analogs. Figure 14 compares the room temperature cell polarization curves and power densities for the hydrogen/oxygen and the methanol/oxygen miniature fuel cells.

Hydrogen fuel cells have very different issues that must be addressed in their construction, but there has been no attempt here to tailor the electrode chips to the different fuel. The presented results show that the m-PEFCs developed in the present investigation could easily be adapted to operate on hydrogen/oxygen.

Conclusions

Microfabrication processes have been successfully used to form miniature fuel cells on a silicon wafer. The processes yielded reproducible, controlled structures that performed well for liquid feed, direct methanol/air systems. The effect of system variables matched that expected from large cells. The etched feed holes (30 μm dia.) handled the flow requirements of liquid feed/gas release at the anode with no evidence of blockage. Since the fabrication can be controlled in a straightforward way, future designs with more sophisticated features could be easily accomplished by changing the mask

Table 3. Large-PEFC vs. *m*-PEFC Test Conditions

Cell	Electrode Area (m^2)	Nafion	CH_3OH Temp. (°C) Conc. (M) Flow Rate (L/min.) Pres. (atm)	Anode Mass Loading (mg/cm^2)	Oxygen Air/O_2 Flow Rate (L/min.) Pres. (atm)	Cathode Mass Loading (mg/cm^2)
Narayanan et al. (2000)	25	117	60 0.5 0.2 1	12	Air 1 2.4	12
Valdez et a. (1999)	80	117	60 0.5 0.2 1	12	Air 1.75 1	12
Whitham et al. (2000)	25	117	90 1.0 (?) 1	0.1	O_2 4 2.4	12
Ren et al. (2000)	5	117	80 0.5 0.0025 1	2	Air 0.6 2.1	1.2
Liu et al. (1998)	5	117	70 0.5 0.025 1	6	O_2 0.4 1.7	6
Baldauf and Preidel (1999)	3	117	80 0.5 (?) 1	1	Air 0.1 1.48	4
Scott et al. (1999)	9	117	70 0.5 0.00136 1	2	Air (?) 1.97	1
Arico et al. (1998)	5	117	95 2.0 (?) 1	1	Air 5	1
Large-PEFC (Kelley et al. 2000)	25	117	70 0.5 0.14 1	4	Air 5 2.4	2.5
m-PEFC (Kelley et al., 2000)	0.25	117	70 0.5 0.2 1	1.28	Air 0.2 1	2.5

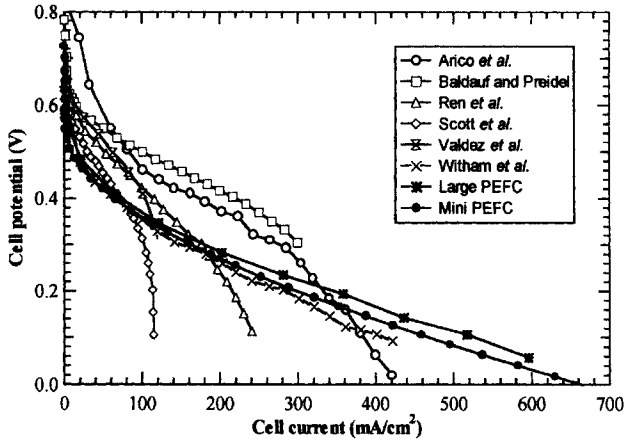

Figure 12. Comparison of results of m-PEFC with large-PEFC Cells (in literature).

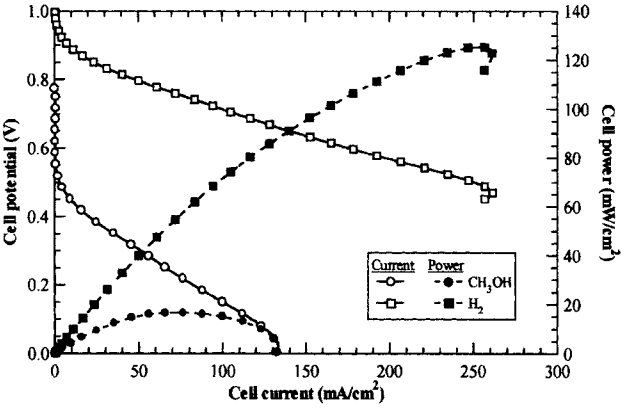

Figure 14. Mini-PEFC methanol/oxygen vs. hydrogen/oxygen cell performance.

23°C; 0.2 L/min. 0.5 M aqueous methanol fuel; 0.2 L/min. 30°C hydrated neat hydrogen; 0.2 L/min. ambient air; Nafion 112.

configuration. Changes of feed hole size or separation distance may improve the behavior of the air cathode structure, for example, to facilitate removal of product water and avoid liquid-phase condensation within the porous electrode structure. This takes advantage of our ability to tailor the holes and ribs to match the needs of individual reactants.

The bipolar cells studied here are simple to form and are robust and reproducible. The volume or mass of the miniature reactor are controlled by the dimensions of the feed hole array of each electrode chip, by the reaction zone of each electrode, and by the thickness of the polymer electrolyte separator. One may scale the system simply by changing the number of feed holes. For example, one may reduce the size of the reactor by three orders of magnitude by reducing the number of holes from 5,184 to 1, and this will change the volume from 0.012 cm^3 to 12×10^{-6} cm^3. Such a change would scale the output current and power as well. At the other extreme, one may scale up by replication of the individual chips. The ability to scale up or down may facilitate integration of sensors and pumps for complete systems.

The porous electrode structure was formed by a simple series of processes that could be adapted to repeatable mass production. The processes are adaptations of procedures that

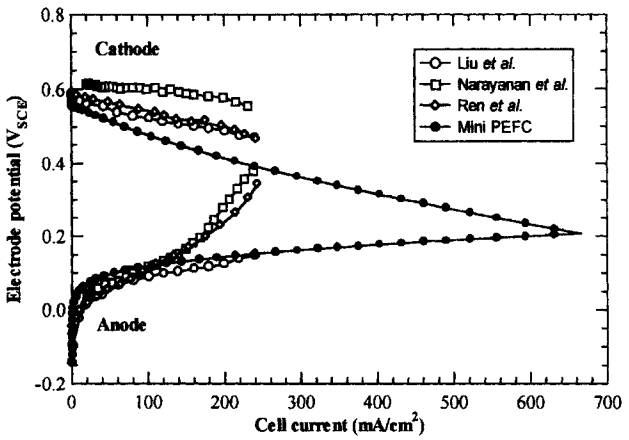

Figure 13. Large-PEFC vs. m-PEFC single electrode performance.

are used to form large cells, with the exception of the electrodeposition of Pt-Ru. The latter process has been studied in previous work published in the literature, but our adaptation of it to the miniature cells has several novel aspects. With this procedure, we have achieved higher catalyst utilization than previously reported. In addition, the size of the reaction zone in the porous electrodes was controlled by the feed hole geometry, as well as by the thickness of the carbon film deposited on the gold current collector surface. The latter dimension was about 2 μm, but the thickness could be changed by altering the spray coating process. Changing the number of feed holes in the electrode chip, as described above, would not affect the spray coating process. Forming several porous electrodes on a single wafer could also be accommodated for series and parallel fuel cell "stacks" by masking, spray deposition of carbon, and electrodeposition of the catalyst. This should lead to higher utilization of materials, and better heat-transfer management, but this needs to be demonstrated.

For many applications that have been proposed for microscale fuel cells, it would be necessary that they be standalone systems with no external pumps or other ancillary devices. In order to deliver the fuels at a desirable rate, natural convection and stirring would be necessary. Air breathing electrodes (cathodes) have been described in the patent literature (Wilson, 1996) for small systems, but these do not approach microscale devices. Air convection is necessary to remove product water from the electrode to prevent liquid-phase condensation within the porous electrode structure that would block access of oxygen to the reaction zone. At room temperature, the present design has been found (data not shown) to support modest cell currents with no artificial pumping. As the temperature rises, however, convective stirring of the air on the backside of the flow manifold is necessary to support the higher currents that can be achieved. It seems likely that smaller and more numerous feed holes on the cathode structure will be necessary to achieve air breathing operation with no artificial augmentation of air delivery. This along with self-heating to about 50–60°C will yield performance of miniature methanol/air fuel cells that could be

attractive for many applications. Applications that seem feasible include power for micro- or nano-sensors, small robots or biomedical devices, or for distributed computing ("smart dust", see, for example, Warneke et al., 2001). The reproducibility of the fabrication processes should shorten the time from laboratory to commercial development. Nevertheless, there remain significant challenges to design and to fabricate complete systems. The present work is one step along the way.

Finally, we will briefly discuss the miniature biofuel cell that was recently described (Chen et al., 2001). The novel cell used enzyme catalysts for glucose oxidation and for oxygen reduction, respectively, and was noted to have 1/60 the size of the present system. The current density and power density (that is, normalized for electrode area) were about 200 times smaller at room temperature and even smaller at elevated temperatures. The present system could be scaled down in size by three orders of magnitude, as noted above, but with no decrease of current density expected.

Literature Cited

Adlhart, O. J., P. Rohonyi, D. Modroukas, and J. Driller, "A Small Portable Proton Exchange Membrane Fuel Cell and Hydrogen Generator for Medical Applications," *ASAIO Journal*, 214 (1997).

Amann, C. A., "Alternative Fuels and Power Systems in the Long Term," *Int. J. of Vehicle Design*, **17**(5/6), 510 (1996).

Appleby, A. J., "Electrochemical Energy-Progress Towards a Cleaner Future: Lead/Acid Batteries and the Competition," *J. of Power Sources*, **53**, 187 (1995).

Arico, A. S., P. Creti, P. L. Antonucci, J. Cho, H. Kim, and V. Antonucci, "Optimization of Operating Parameters of a Direct Methanol Fuel Cell and Physico-Chemical Investigation of Catalyst-Electrolyte Interface," *Electrochimica Acta*, **43**(24), 3719 (1998).

Baldauf, M., and W. Preidel, "Status of the Development of a Direct Methanol Fuel Cell," *J. of Power Sources*, **84**, 161 (1999).

Barton, S. C., T. F. Fuller, and A. C. West, *Electrode Design for Strip-Cell Direct Methanol Fuel Cells*, Vol. 98-2, Abst. 1089, The Electrochem. Society, Inc., Pennington, NJ (1998a).

Barton, S. A. C., B. L. Murach, T. F. Fuller, and A. C. West, "A Methanol Sensor for Portable Direct Methanol Fuel Cells," *J. of Electrochem. Soc.*, **145**(11), 3783 (1998b).

Bates, J. B., N. J. Dudney, D. C. Lubben, G. R. Gruzalski, B. S. Kwak, X. Yu, and R. A. Zuhr, "Thin-Film Rechargeable Lithium Batteries," *J. of Power Sources*, **54**, 58 (1995).

Bean, K. E., "Anisotropic Etching of Silicon," *IEEE Trans. on Electron Devices*, **25**(10), 1185 (1978).

Belyi, V. I., *Silicon Nitride in Electronics*, Materials Science Monographs, ed. 34, Elsevier, New York (1988).

Brown, C. J., D. Pletcher, F. C. Walsh, J. K. Hammond, and D. Robinson, "Local Mass Transport in the FM01 Laboratory Electrolyser," *J. of Appl. Electrochemistry*, **22**, 613 (1992).

Büchler, M., S. C. Kelley, and W. H. Smyrl, "Scanning Electrochemical Microscopy with Shear Force Feedback: Investigation of the Lateral Resolution of Different Experimental Configurations," *Electrochem. and Solid-State Lett.*, **3**(1), 35 (2000).

Burns, J. R. and C. Ramshaw, "Development of a Microreactor for Chemical Production," *Chemical Eng. Res. and Des.*, **77**(3), 206 (1999).

Burns, M. A., B. N. Johnson, S. N. Brahmasandra, K. Handique, J. R. Webster, M. Krishnan, T. S. Sammarco, P. M. Man, D. Jones, D. Heldsinger, C. H. Mastrangelo, and D. T. Burke, "An Integrated Nanoliter DNA Analysis Device," *Science*, **282**, 484 (1998).

Campbell, S. A., *The Science and Engineering of Microelectronic Fabrication*, Oxford University Press, New York (1996).

Chambers, R. D., and R. C. H. Spink, "Microreactors for Elemental Fluorine," *Chem. Commun.*, 883 (1999).

Chen, T., S. Calabrese-Barton, G. Binyamin, Z. Gao, Y. Zhang, H-H. Kim, and A. Heller, "A Miniature Biofuel Cell," *J. Am. Chem. Soc.*, **123**, 8630 (2001).

Cho, B.-O., S.-W. Hwang, I.-W. Kim, and S. H. Moon, "Expression of the Si Etch Rate in a CF_4 Plasma with Four Internal Process Variables," *J. of Electrochem. Soc.*, **146**(1), 350 (1999).

Cleghorn, S. J. C., C. R. Derouin, M. S. Wilson, and S. Gottesfeld, *A Printed Circuit Board Approach to Measuring Current Distribution in a Fuel Cell*, Vol. 96-2, Abst. 798, The Electrochemical Society, Inc., (1996).

Datta, M., and N. Smilanich, *National Electronics Manufacturing Technology Roadmaps*, National Electronics Manufacturing Initiative, Inc. (1996).

DeWitt, S. H., "Microreactors for Chemical Synthesis," *Current Opinion in Chemical Biology*, **3**, 350 (1999).

Dyer, C. K., "A Novel Thin-Film Electrochemical Device for Energy Conversion," *Nature*, **343**, 547 (1990).

Ehrfeld, W., F. Golbig, V. Hessel, H. Lowe, and T. Richter, "Characterization of Mixing in Micromixers by a Test Reaction: Single Mixing Units and Mixer Arrays," *Indust. Eng. Chem. Res.*, **38**, 1075 (1999).

Gojkovic, S. L., S. Gupta, and R. F. Savinell, "Heat-Treated Iron(III) Tetramethyoxyphenyl Porphyrin Chloride Supported on High-Area Carbon as an Electrocatalyst for Oxygen Reduction Part II. Kinetics of Oxygen Reduction," *J. of Electroanalytical Chemistry*, **462**, 63 (1999).

Gojkovic, S. L., S. Gupta, and R. F. Savinell, "Heat-Treated Iron(III) Tetramethoxyphenyl Porphyrin Chloride Supported on High-Area Carbon as an Electrocatalyst for Oxygen Reduction: Part III. Detection of Hydrogen-Peroxide during Oxygen Reduction," *Electrochimica Acta*, **45** 889 (1999).

Gottesfeld, S. and M. W. Wilson, "Polymer Electrolyte Fuel Cells as Potential Power Sources for Portable Electronic Devices," *Energy Storage Systems for Electronics*, T. Osaka and M. Datta, eds., Gordon & Breach Science Publishers, New York, p. 487 (2000).

Gupta, S., D. Tryk, S. K. Zecevic, W. Aldred, D. Guo, and R. F. Savinell, "Methanol-Tolerant Electrocatalysts for Oxygen Reduction in a Polymer Electrolyte Membrane Fuel Cell," *J. of Appl. Electrochemistry*, **28**, 673 (1998).

He, B., L. Tan, and F. Regnier, "Microfabricated Filters for Microfluidic Analytical Systems," *Analytical Chemistry*, **71**, 1464 (1999).

Hebling, C., *Small Fuel Cells*, Proceedings Volume, Knowledge Foundation, New Orleans (Apr. 2000).

Hecht, A. M., *Small Fuel Cells*, Proceedings Volume, Knowledge Foundation, New Orleans (Apr. 2000).

Heinzel, A., R. Nolte, K. Ledjeff-Hey, and M. Zedda, "Membrane Fuel Cells-Concepts and System Design," *Electrochimica Acta*, **43**(24), 3817 (1998).

Hsing, I. M., R. Srinivasan, M. P. Harold, K. F. Jensen, and M. A. Schmidt, "Simulation of Micromachined Chemical Reactors for Heterogeneous Partial Oxidation Reactions," *Chem. Eng. Sci.*, **55**, 3 (2000).

Jensen, K. F., "Microchemical Systems: Status, Challenges, and Opportunities," *AIChE J.*, **45**(10), 2051 (1999).

Jones, S. D., J. R. Akridge, and F. K. Shokoohi, "Thin Film Rechargeable Li Batteries," *Solid State Ionics*, **69**, 357 (1994).

Kelley, S. C., G. A. Deluga, and W. H. Smyrl, "A Miniature Methanol/Air Polymer Electrolyte Fuel Cell," *Electrochemical and Solid-State Letters*, **3**(9), 407 (2000).

Kenis, P. J. A., R. F. Ismagilov, and G. M. Whitesides, "Microfabrication Inside Capillaries Using Multiphase Laminar Flow Patterning," *Science*, **285**, 83 (1999).

Kostecki, R., X. Song, and K. Kinoshita, "Electrochemical Analysis of Carbon Interdigitated Microelectrodes," *Electrochemical and Solid-State Letters*, **2**(9), 465 (1999).

Kovacs, G. T. A., C. W. Storment, M. Carl R. Halks-Miller, J. Belczynski, C. C. D. Santina, E. R. Lewis, and N. I. Maluf, "Silicon-Substrate Microelectrode Arrays for Parallel Recording of Neural Activity in Peripheral and Cranial Nerves," *IEEE Trans. on Biomed. Eng.*, **41**(6), 567 (1994).

Lee, S. J., F. B. Prinz, S. W. Cha, and Y. C. Liu, "High Power Density Polymer Electrolyte Fuel Cells by Microfabrication," Abstract 57, Toronto Meeting Society, (May 2000).

Lee, S. J., S. W. Cha, Y. Liu, R. O'Hayre, A. Chang-Chen, and F. B. Prinz, "Miniature Fuel Cells with Non-Planar Interface by Microfabrication," Abstract 241, Phoenix Meeting Electrochemical Society, (Oct. 2000).

Li, N., C. R. Martin, and B. Scrosati, "A High-Rate, High-Capacity, Nanostructured Tin Oxide Electrode," *Electrochemical and Solid-State Letters*, **3**(7), 316 (2000).

Liu, L., C. Pu, R. Viswanathan, Q. Fan, R. Liu, and E. S. Smotkin, "Carbon Supported and Unsupported Pt-Ru Anodes for Liquid Feed Direct Methanol Fuel Cells," *Electrochimica Acta*, **43**(24), 3657 (1998).

Matsuoka, M., Y. Yoshida, and M. Moronuki, "Preparation of Silicon Thin Diaphragms Free from Micopyramids Using Anisotropic Etching in KOH Solutions," *J. of Chem. Eng. Japan*, **25**(6), 735 (1992).

Maynard, H., and J. P. Meyers, *Small Fuel Cells*, Proceedings Volume, Knowledge Foundation, New Orleans (Apr. 2000).

Maynard, H., J. Meyers, and A. Glebov, "Silicon Tunnels for Reactant Distribution in Miniaturized Fuel Cells," Abstract 60, Toronto Meeting, Electrochemical Society (May 2000).

Meyers, J., and H. Maynard, "Design of Miniaturized Fuel Cells for Portable Power," Abstract 64, Toronto Meeting Electrochemical Society (May 2000).

Narayanan, S. R., T. I. Valdez, and W. Chun, "Design and Operation of an Electrochemical Methanol Concentration Sensor for Direct Methanol Fuel Cell Systems," *Electrochem. and Solid-State Lett.*, **3**(3), 117 (2000).

Parthasarathy, A., C. R. Martin, and S. Srinivasan, "Investigations of the O_2 Reduction Reaction at the Platinum/Nafion Interface Using a Solid-State Electrochemical Cell," *J. of Electrochem. Soc.*, **138**(4), 916 (1991).

Patankar, N. A., and H. H. Hu, "Numerical Simulation of Electroosmotic Flow," *Analytical Chemistry*, **70**, 1870 (1998).

Petersen, K. E., "Silicon as a Mechanical Material," *Proc. of IEEE*, **70**(5), 420 (1982).

Powers, R. A., "High Performance Polymers: Their Origin and Development," *Proc. of IEEE*, **83**(4), 687 (1995).

Ren, X., T. E. Springer, and S. Gottesfeld, "Water and Methanol Uptakes in Nafion Membranes and Membrane Effects on Direct Methanol Cell Performance," *J. Electrochem. Soc.*, **147**(1), 92 (2000).

Ren, X., M. S. Wilson, and S. Gottesfeld, *Proton Conducting Membrane Fuel Cells I*, S. Gottesfeld, G. Halpert, and A. Landgrebe, eds., PV 95-23, 252, the Electrochemical Society Proceedings Series, Pennington, NJ (1995).

Rieke, P. C., and N. E. Vanderborgh, "Thin Film Electrode Arrays for Mapping the Current-Voltage Distributions in Proton-Exchange-Membrane Fuel Cells," *J. of the Electrochem. Soc.*, **134**(5), 1099 (1987).

Ristic, L., H. Hughes, and F. Shemansky, "Bulk Micromachining Technology," *Sensor Technology and Devices*, Chapter 3, L. Ristic, ed., Artech Hous, Boston, 49 (1994).

Santini, J. T., M. J. Cima, and R. Langer, "A Controlled-Release Microchip," *Nature*, **397**, 335 (1999).

Savinell, R., J. Wainright, L. Dudik, K. Yee, L. Chen, C. C. Liu, Y. Zhang, and M. Litt, "Microfabricated Fuel Cells for Portable Power," Abstract 63, Toronto Meeting, Electrochemical Society (May 2000).

Scott, K., W. M. Taama, P. Argyropoulos, and K. Sundmacher, "The Impact of Mass Transport and Methanol Crossover on the Direct Methanol Fuel Cell," *J. of Power Sources*, **83**, 204 (1999).

Srinivasan, R., I.-M. Hsing, P. E. Berger, K. F. Jensen, S. L. Firebaugh, M. A. Schmidt, M. P. Harold, J. J. Lerou, and J. F. Ryley, "Micromachined Reactor for Catalytic Partial Oxidation Reactions," *AIChE J.*, **43**(11), 3059 (1997).

Sun, G. Q., J. T. Wang, and R. F. Savinell, "Iron(III) tetramethoxyphenylporphyrin(FeTMPP) as Methanol Tolerant Electrocatalyst for Oxygen Reduction in Direct Methanol Fuel Cells," *J. of Appl. Electrochemistry*, **28**, 1087 (1998).

Surampudi, S., H. A. Frank, S. R. Narayanan, W. Chun, B. Jeffries-Nakamura, A. Kinder, and G. Halpert, U.S. Patent No. 5,773,162 (1998).

Tokumitsu, K., J. S. Wainright, and R. F. Savinell, "Electrochemical Properties of Platinum/Carbon Ink Electrodes for Direct Methanol Polymer Electrolyte Fuel Cells," *J. of New Materials for Electrochem. Systems*, **2**, 171 (1999).

Valdez, T. I., and S. R. Narayanan, *Recent Studies on Methanol Crossover in Liquid-Feed Direct Methanol Fuel Cells*, Vol. 98-2, Abst. 1123, The Electrochemical Society, Inc., Pennington, NJ (1998).

Valdez, T. I., *Testing of a Five-Cell Liquid-Feed Direct Methanol Fuel Cell Stack for a 15-Watt System*, Vol. 99-2, Abst. 410, The Electrochemical Society, Inc., Pennington, NJ (1999).

Vincent, C. A., and B. Scrosati, *Modern Batteries: An Introduction to Electrochemical Power Sources*, 2nd ed., J. Wiley, New York (1997).

Wainright, J. S., K. Yee, M. H. Litt, Y. Zhang, C. C. Liu, and R. F. Savinell, "A Microfabricated Hydrogen/Air Fuel Cell Incorporating a Novel Polymer Electrolyte," Abstract 234, Phoenix Meeting Electrochemical Society (Oct. 2000).

Walker, P., and W. H. Tarn, eds., *CRC Handbook of Metal Etchants*, CRC Press, Boca Raton, FL (1991).

Warneke, B., M. Last., B. Liebowitz, and K. S. J. Pister, *Computer*, 44 (Jan. 2001).

Whitham, C. K., W. Chun, T. I. Valdez, and S. R. Narayanan, "Performance of Diret Methanol Fuel Cells with Sputter-Deposited Anode Catalyst Layers," *Electrochem. and Solid-State Lett.*, **3**(11), 497 (2000).

Wieser, C. H., A. Helmbold, and W. Wchnurnberger, *Advanced Method to Measure Current Gradients in Polymer Electrolyte Fuel Cells*, Vol. 98-2, Abst. 1115, The Electrochemical Society, Inc., Pennington, NJ (1998).

Wilson, M. S., U.S. Patent No. 5514486 (1996).

Xia, Y., and G. M. Whitesides, "Soft Lithography," *Ann. Rev. on Mat. Sci.*, **28**, 153 (1998).

Manuscript received June 22, 2001, and revision received Oct. 23, 2001.